Grain size sorting over offshore sandwaves: observations and modelling

Pieter C. Roos, Suzanne J.M.H. Hulscher, Fenneke van der Meer
Water Engineering and Management, University of Twente, Enschede, The Netherlands

Thaiënne A.G.P. van Dijk
TNO Built Environment and Geosciences – Geological Survey of the Netherlands, Utrecht, The Netherlands

Irene G.M. Wientjes
Institute for Marine and Atmospheric Research, Utrecht University, Utrecht, The Netherlands

Joris van den Berg
Numerical Analysis and Computational Mechanics, University of Twente, Enschede, The Netherlands

Offshore sandwaves are rhythmic bed patterns widely present in shallow shelf seas. Observations from the North Sea indicate a trend of coarser sediment with a higher sorting at sandwave crests. In this study, we present an extended model for sandwave dynamics that accounts for the presence and transport of non-uniform sediment. The extension involves an active layer as well as a fractional calculation of sediment transport, which includes hiding-exposure effects. Simulations of a growing sandwave for a bimodal mixture indicate a coarsening trend towards the crest, whereas in the sandwave troughs the sediment remains mixed. The model results show qualitative agreement with observations from various sites in the North Sea.

1 INTRODUCTION

Offshore sandwaves are rhythmic bed patterns widely present in shallow seas like the North Sea. They are characterized by wavelengths of the order of hundreds of meters and heights that may exceed 10 m (Passchier and Kleinhans 2005). Depending on the tidal flow conditions, tidal sandwaves can migrate up to tens of meters per year (Van Dijk and Kleinhans 2005; Van Dijk et al. 2006). Due to their dimensions and dynamic behaviour, tidal sandwaves may interfere with e.g. navigation, pipelines and offshore constructions. Improving our insight in the dynamics of tidal sandwaves is therefore not only of theoretical, but also of practical relevance.

Morphodynamic models have been developed to investigate, simulate and predict sandwave dynamics. Using linear stability analysis, the formation of tidal sandwaves has been explained as an inherent instability of a flat sandy seabed subject to tidal flow (Hulscher 1996). Subsequently, nonlinear numerical studies were carried out to investigate the finite amplitude evolution of tidal sandwaves towards an equilibrium shape (Van den Berg and Van Damme 2005; Németh et al. 2007). A common feature of the morphodynamic models is that all are idealized, i.e. with strongly simplified representations of geometry, hydrodynamics and sediment transport. For example, in each of the existing sandwave models the sediment is assumed to be of uniform size. However, observations from various locations in the North Sea indicate that grain sizes vary over tidal sandwaves (Schüttenhelm 2002; Passchier and Kleinhans 2005), which cannot be described nor explained by the existing sandwave models. The goal of this study is to explain empirical grain size patterns over tidal sandwaves, by developing an extended sandwave simulation model.

To this end, we first give an overview of grain size patterns over tidal sandwaves as observed at various locations in the Southern North Sea (Section 2). In Section 3, we present a morphodynamic sandwave model that accounts for the presence and transport of non-uniform sediment. It is based on an existing nonlinear numerical sandwave simulation model (Van den Berg and Van Damme 2005), which we have extended in the following respects: the introduction of an active layer (Hirano 1971) and a fractional calculation of sediment transport, including hiding-exposure effects; e.g. see Seminara (1995). Section 4 contains the model results, obtained when introducing a bimodal sediment mixture with coarse and fine grains.

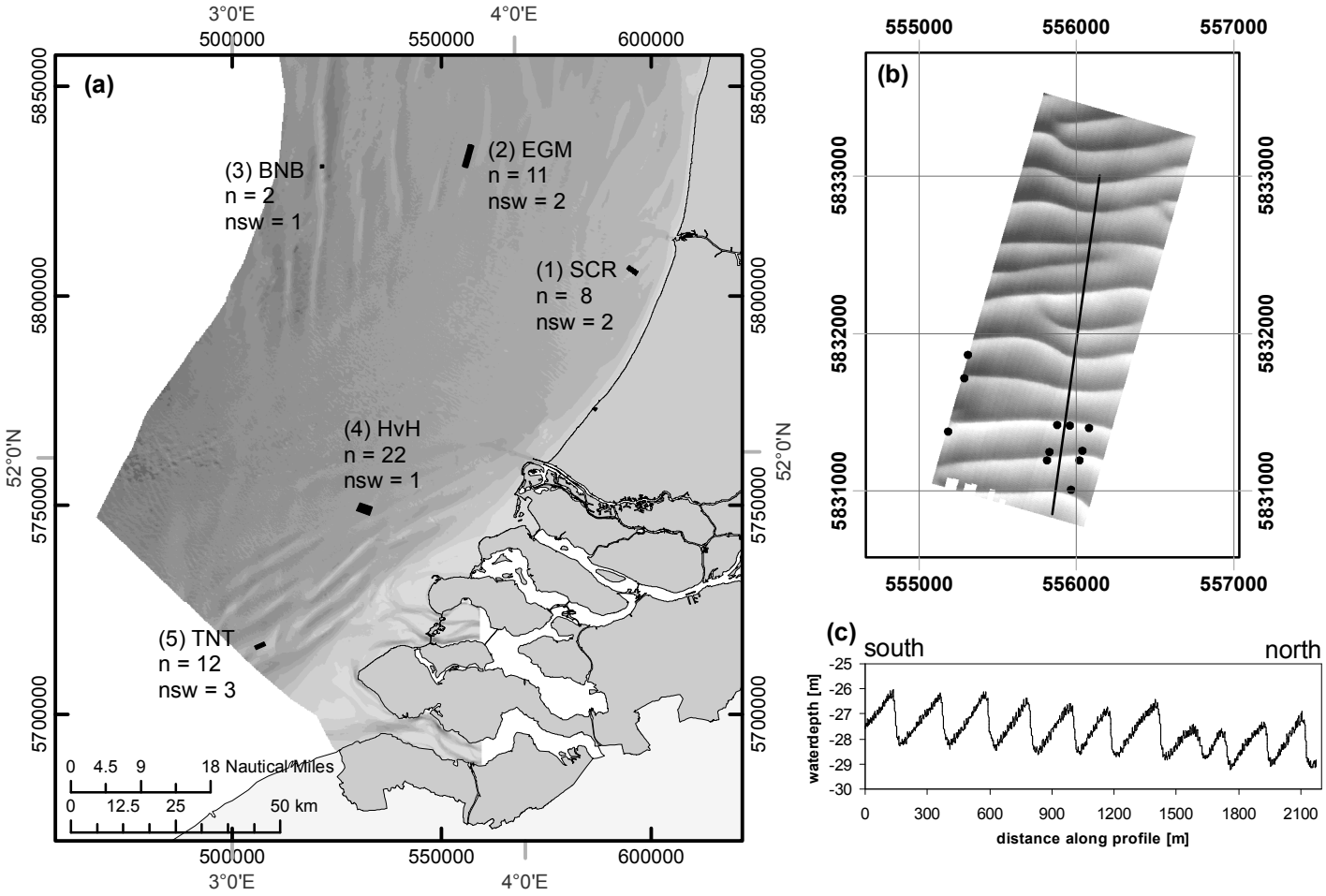

Figure 1: (a) Location map of study sites with bathymetry in the southern North Sea, with n the number of samples per site and nsw the number of sandwaves covered by the sampling. (b) Multibeam echo sounding image of site 2 with sample locations and (c) a cross-sectional profile.

In Section 5, the results are discussed, also in comparison to the observations from the North Sea. Finally, Section 6 contains the conclusions.

2 OBSERVATIONS FROM THE NORTH SEA

2.1 *Data collection and processing*

Grain size variability over sandwaves is observed at several locations of different water depths, sandwave morphology and flow conditions in the North Sea. At five sites, sampling strategies were especially designed to record grain size patterns over sandwaves. Samples were taken at crests, in troughs and in most cases also on the slopes of sandwaves (Figure 1). Sea bed sampling was carried out using a cylindrical box corer, of which sediment cores were resampled on board, except for site 4, where a vibrocorer was used. Grain size distributions of sea bed subsamples were determined in the lab by laser diffraction, using a Malvern 2000, for grain sizes smaller than 2 mm after sieving off the coarser material. All samples fall within the sand fraction, i.e. noncohesive sediment. The sandwaves at all sites are compound sandwaves, i.e. sandwaves with superimposed megaripples. They furthermore display migration, with migration rates that differ from site to site.

2.2 *Site-specific characteristics*

Site 1 is a coastal site near Zandvoort, where three-dimensional sandwaves are superimposed on and restricted to a shoreface-connected ridge ('SCR'). These sandwaves are asymmetric in cross-sectional profile, with their lee slopes facing north-east. Water depths at this site range from 14 m on top of the ridge to 18.3 m in the adjacent swales. The one sandwave that is fully covered with multibeam echo sounding measurements has a wavelength of 760 m and a wave height of 1.5 m. In contrast with sandwaves in other locations, these have flattened crest plateaus. Median grain sizes (D_{50}) at the crest plateaus range from 340 to 350 μm between samples; sorting ratios (D_{60}/D_{10}) are 1.47 or 1.48. Median grain sizes in the troughs vary between 219 and 327 μm and sorting ratios are similar to those at the crests, 1.48 and 1.49 (March 2001).

Site 2 is a sandwave field 50 km offshore of Egmond aan Zee ('EGM') and comprises straight, asymmetrical sandwaves (see Figure 1b and c) with an average wavelength of 203 m, an average wave

Table 1: Bathymetric*, morphologic† and sedimentologic‡ characteristics of the five North Sea sites in Figure 1.

site	H [m]	$L_{sw,avg}$ [m]	$H_{sw,avg}$ [m]	$D_{50,cr}$ [μm]	$D_{50,tr}$ [μm]	$D_{50,sl}$ [μm]	$(D_{60}/D_{10})_{cr}$ [$-$]	$(D_{60}/D_{10})_{tr}$ [$-$]	$(D_{60}/D_{10})_{sl}$ [$-$]
(1) SCR	14-18	760	1.5	342-351	319-321	323-360	1.47-1.48	1.48-1.49	1.47-1.49
(2) EGM	26-30	203	1.8	273-297	254-272	.	1.48-1.54	1.53-1.54	.
(3) BNB	17-44	206	2.5	314	316	.	1.44	1.46	.
(4) HvH	19-28	350	7.3	396-561	303-461	370-506	1.54-1.77	1.55-1.80	1.55-1.63
(5) TNT	11-37	145	3.9	397-421	436-530	378-551	1.56-1.69	1.61-13.3	1.62-10.5

*Approximate range in water depth; †average sandwave length $L_{sw,avg}$ and height $H_{sw,avg}$; ‡median grain size D_{50} and sorting ratios D_{60}/D_{10}, for the crests ('cr'), the troughs ('tr') and the slopes ('sl'), respectively.

height of 1.8 m and their lee slopes facing north-northeast (Van Dijk and Kleinhans 2005). Here, water depths range from 26 to 30 m. Median grain sizes (June 2001) vary from 273 to 297 μm at the crests and from 254 to 272 μm in the troughs. Sorting ratios are 1.48 to 1.54 (only one of 1.54) at the crests and 1.53 to 1.54 in the troughs.

Site 3 comprises offshore sandwaves on a tidal ridge, the Brown Bank ('BNB'), where water depths vary between 17 m at the top of the ridge and 44 m in the swales. Here, sandwaves are asymmetrical with their lee sides facing northeast and have an average wavelength of 206 m and an average wave height of 2.5 m. Only one sand wave was sampled at this site (November 2006), resulting in a median of 314 μm at the crest and 316 μm in the trough. The sorting ratios are 1.44 and 1.46 at the crest and in the trough, respectively.

Site 4 is located 45 km west-southwest of Hoek van Holland ('HvH'), where sandwaves are more symmetric and have steeper sides and wide gentle troughs. Area-covering multibeam echo soundings of one sandwave show that its wavelength is approximately 350 m and its wave height is up to 7.3 m. Water depths range from 19 to 28 m. Median grain sizes (April 2001) vary from 396 to 561 μm at the crest and from 303 to 461 μm in the troughs. Sorting ratios are between 1.54 and 1.77 at the crest and between 1.55 and 1.80 in the troughs (Schüttenhelm 2002).

Site 5 reveals sandwaves on a tidal ridge Thornton Bank ('TNT'), where water depths range from 11 m over the bank to 37 m in the swales. The sandwaves are symmetric in cross-sectional profile and have relatively steep slopes. Their average wavelength is 145 m and their heights are 1.0 to 6.9 m, with an average of 3.9 m. Median grain sizes at the sandwave crests (October 2006) range from 397 to 421 μm and in the troughs from 436 to 530 μm. Sorting ratios are 1.56 to 1.69 at the crests and 1.61 to an exceptional 13.3 in the troughs. In general, grain sizes show more variability than at the other sites.

An overview of bathymetric, morphologic and sedimentologic characteristics is provided in Table 1. The sandwave dimensions at sites 1, 2, 3 and 5 have been calculated with a semi-automated method (Van Dijk et al. 2006) from digital multibeam echo soundings; at site 4 this was done manually.

2.3 *Conclusions on observed sorting patterns*

The existence of grain size variability patterns over sandwaves is evident from the clustering in grain size characteristics per morphological unit of sandwaves (Figure 2). Although exceptions exist and grain size variability over sandwaves may be less clear per season at sites where sampling was done in seasonal time series, grain size differences between crests and troughs of offshore sandwaves, although subtle, show a general trend of coarser and well-sorted sediments (lower sorting ratios) at the sandwave crests and finer-grained and less well-sorted sediments in the troughs (Figure 2).

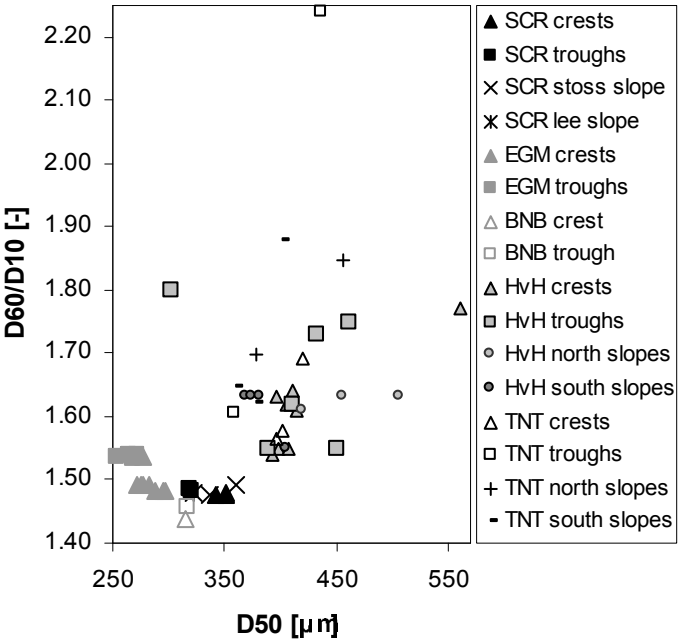

Figure 2: Bivariate plot of the median grain size D_{50} versus a sorting ratio, D_{60}/D_{10}, per morphological sandwave unit for five study sites in the North Sea. Two extreme data points of site 5 (TNT, see Table 1) fall outside the plot.

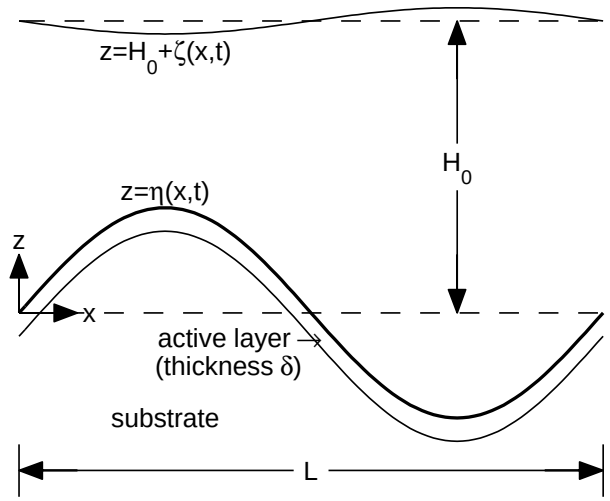

Figure 3: Definition sketch of model geometry, for clarity strongly exaggerating the vertical scale and the active layer thickness.

3 MORPHODYNAMIC MODEL

3.1 *Geometry*

Consider a two-dimensional coordinate system with a horizontal x-axis, and a vertical z-axis pointing upward (with $z = 0$ denoting the spatial average of the bed level). The sea bed is located at $z = \eta(x, t)$, which defines the top of a so-called active layer to be introduced below. The free surface is at $z = \zeta(x, t) + H_0$ where the constant H_0 represents the undisturbed water depth (here: $H_0 = 30$ m).

The flow velocity is represented by the vector quantity $\boldsymbol{u} = (u, w)$, with components in x- and z-direction respectively. Regarding the horizontal coordinate we assume spatial periodicity, effectively imposing the wavelength L of the sandwaves, which is then kept constant throughout each morphodynamic simulation. See Figure 3 for a sketch.

3.2 *Hydrodynamics and solution method*

The hydrodynamic module is based on the 2DV-shallow water equations (assuming hydrostatic pressure) and with a Boussinesq turbulence closure involving a constant value of the vertical eddy viscosity $A_{\text{v}} = 0.03$ m^2 s^{-1}. Kinematic boundary conditions are imposed at the free surface and at the sea bed. Furthermore, dynamic boundary conditions require zero stress at the free surface and partial slip at the bed, with slip parameter $S = 0.01$ m s^{-1}. A time-dependent body force is added to the momentum equations in order to mimic the forcing that drives the tidal flow in the domain. This forcing is chosen such that, over a flat bed, it induces a sinusoidal tidal flow with a depth-averaged peak value of 1 m s^{-1} and a period of 12.42 hrs (M2-component). More details on the hydrodynamic model formulation as well as the numerical solution procedure can be found in Van den Berg and Van Damme (2005).

For a given bed profile η, the main output of the hydrodynamic module is the bed shear stress:

$$\tau_{\text{b}}(x,t) = \rho A_{\text{v}} \left.\frac{\partial u}{\partial z}\right|_{z=\eta}. \tag{1}$$

This quantity, varying over the domain and within the tidal cycle, is then used as input for the sediment transport module.

3.3 *Sediment, active layer and bed evolution*

We consider a noncohesive sediment mixture that consists of N distinct fractions of grain size D_j ($j = 1, 2, \ldots, N$). Following Hirano (1971), the sea bed is divided into an active layer of constant and uniform thickness δ (located at $\eta - \delta \leq z \leq \eta$) and a substrate ($z < \eta - \delta$; see Figure 3). Each of these layers is characterized by volume fractions for the grain size classes j: $F_j(x, t)$ in the active layer, which may vary in space and time; $F_{\text{substr},j}$ for the substrate, assumed uniform and constant. By definition, these fractions must add up to 1, i.e. $\sum_j F_j = 1$ and $\sum_j F_{\text{substr},j} = 1$ (all summations from $j = 1$ to $j = N$). Moreover, the mean grain size in the active layer is given by $D_{\text{m}} = \sum_j F_j D_j$. By assuming a constant and uniform active layer thickness, we ignore situations in which a non-erodible substrate is locally exposed at the sea bed ($\delta = 0$).

Only the active layer contains material directly available for transport. By moving up and down, the active layer interacts with the substrate. For example, deposition implies an increase of the bed level in time. In turn, the active layer (of constant thickness δ) shifts upward, which implies a vertical exchange of sediment from the active layer into the substrate. Conversely, erosion shifts the active layer downward, implying a sediment exchange from substrate into the active layer. This is the indirect mechanism by which the substrate may interact with the flow, sediment transport and bed evolution.

With q_j denoting the volumetric bed load sediment flux (in m^2 s^{-1}) of sediment fraction j in the x-direction and $\langle q_j \rangle$ its tidally averaged value, sediment fraction j satisfies the following conservation law (Seminara 1995):

$$\delta \frac{\partial F_j}{\partial t} + F_{\text{vert},j} \frac{\partial \eta}{\partial t} = \frac{-1}{1-p} \frac{\partial \langle q_j \rangle}{\partial x}, \tag{2}$$

with porosity $p = 0.4$. The volume fractions $F_{\text{vert},j}$ associated with the vertical sediment exchange between active layer and substrate (as explained above) are given by

$$F_{\text{vert},j} = \begin{cases} F_j & \text{if } \partial\eta/\partial t > 0, \\ F_{\text{substr},j} & \text{if } \partial\eta/\partial t < 0. \end{cases} \tag{3}$$

Therefore, also the vertical exchange fractions add up to 1. Summation of the conservation law (2) now leads to an overall sediment balance

$$\frac{\partial \eta}{\partial t} = \frac{-1}{1-p} \frac{\partial \langle q_{\text{tot}} \rangle}{\partial x}, \qquad q_{\text{tot}} = \sum_{j=1}^{N} q_j, \tag{4}$$

which expresses the local bed change $\partial \eta / \partial t$ in terms of the divergence of the (tidally averaged) total sediment flux.

3.4 *Fractional sediment transport*

The fractional sediment flux q_j is calculated from a modified version of the Meyer-Peter & Müller formula (Van Rijn 1993), accounting for bed slope effects:

$$\frac{q_j}{\sqrt{g(s-1)D_{\text{m}}^3}} = 8F_j \left(|\theta_j| - \theta_{\text{cr},j}\right)^{\frac{3}{2}} \left(\frac{\tau_{\text{b}}}{|\tau_{\text{b}}|} - \frac{1}{\mu_{\text{s}}} \frac{\partial \eta}{\partial x} \right), \tag{5}$$

for conditions above the threshold of transport ($|\theta_j| > \theta_{\text{cr},j}$) and $q_j = 0$ otherwise. Here, $\theta_j = \tau_{\text{b}} / [\rho(s-1)gD_j]$ is the Shields parameter and $\theta_{\text{cr},j}$ the critical Shields stress, both for class j. The latter is expressed as a correction to the critical Shields parameter $\theta_{\text{cr,m}}$ (based on the mean grain size), with a so-called hiding-exposure coefficient ξ_j:

$$\theta_{\text{cr},j} = \xi_j \theta_{\text{cr,m}}, \qquad \xi_j = \left[\frac{\log 19}{\log \left(19 D_j / D_{\text{m}}\right)} \right]^2. \tag{6}$$

This formulation, proposed by Egiazaroff (1965), describes the hiding-exposure mechanism experienced by grains in a sediment mixture. In the presence of finer grains, coarser grains protrude relatively further into the flow and are therefore more easily transported than in a situation with uniform sediment: exposure ($\xi_j < 1$, thus reducing the threshold for initiation of sediment transport). Conversely, fine grains hide behind and between coarser grains and are therefore less easily transported: hiding ($\xi_j > 1$, increasing the threshold).

The critical Shields parameter $\theta_{\text{cr,m}}$, based on the mean grain size, is given by (Soulsby 1997)

$$\theta_{\text{cr,m}} = \frac{0.24}{D_{\text{m}}^*} + 0.055 \left[1 - \exp\left(0.02 D_{\text{m}}^*\right)\right], \tag{7}$$

with dimensionless grain size $D_{\text{m}}^* = [g(s-1)/\nu^2]^{1/3} D_{\text{m}}$. The remaining parameters in equations (5) and (7) are the specific gravity of sediment $s = 1.65$, the gravitational acceleration $g = 9.81$ m s^{-2}, a coefficient of static friction $\mu_{\text{s}} = 0.3$, and (in the definition of D_{m}^*) the kinematic viscosity of water $\nu = 1.36 \cdot 10^{-6}$ m^2 s^{-1}.

3.5 *Solution procedure*

For a given bed profile η, the bed shear stress τ_{b} is known from the hydrodynamic module. For each sediment class j, the transport formula (5) is then used to obtain the (tidally averaged) fractional sediment transport $\langle q_j \rangle$, as a function of space.

Next, from the overall sediment balance (4) the local bed change $\partial \eta / \partial t$ is obtained. The sign of this quantity particularly shows whether, locally, sedimentation or erosion occurs. This result is required to determine the local exchange fractions $F_{\text{vert},j}$ from equation (3). The individual sediment balances (2) then provide $\partial F_j / \partial t$, i.e. the evolution of the individual fractions in time. For details on the numerical discretization of the sediment transport module, we refer to Wientjes (2006).

4 RESULTS

4.1 *Overview of simulations*

In the following, we present the results obtained with the morphodynamic model. We particularly focus on the influence of the parameters that characterize the composition of the sediment mixture. To this end, we introduce a bimodal sediment mixture, consisting of coarse and fine grains (Section 4.2). Next, a second simulation is carried out, in which we consider the more simple situation of uniform sediment (Section 4.3). These two simulations allow us to investigate the effect of the non-homogeneity of the sediment mixture. To study the sensitivity of the model results, we finally make runs in which the bimodal sediment composition is further modified (Section 4.4).

All model parameter values are as specified in Section 3. We do not attempt to investigate the model's sensitivity to e.g. the slip parameter, the mean water depth and the tidal flow characteristics. The wavelength L is estimated such that, for small amplitude, the growth rate of the corresponding sandwave is strongest (fastest growing mode). For the reference simulation, this procedure leads to $L = 650$ m. Although the fastest growing mode may shift when a different sediment mixture is considered, it turns out that this dependency of the preferred wavelength on the sediment mixture is rather weak.

The sea bed profile $z = \eta$ at $t = 0$, i.e. the initial topography, is chosen sinusoidal with wavelength L and a small amplitude that is 1% of the mean water depth H_0 (here: 0.3 m). The instability mechanism will cause the bed feature to grow in time and to develop into a sandwave (Hulscher 1996).

4.2 *Simulation with a bimodal mixture*

We consider a bimodal mixture ($N = 2$) with the following grain sizes, labeled 'coa' (coarse) and 'fi' (fine): $D_{\text{coa}} = 400$ μm, $D_{\text{fi}} = 200$ μm, which agrees with the observed grain sizes as reported in Sec-

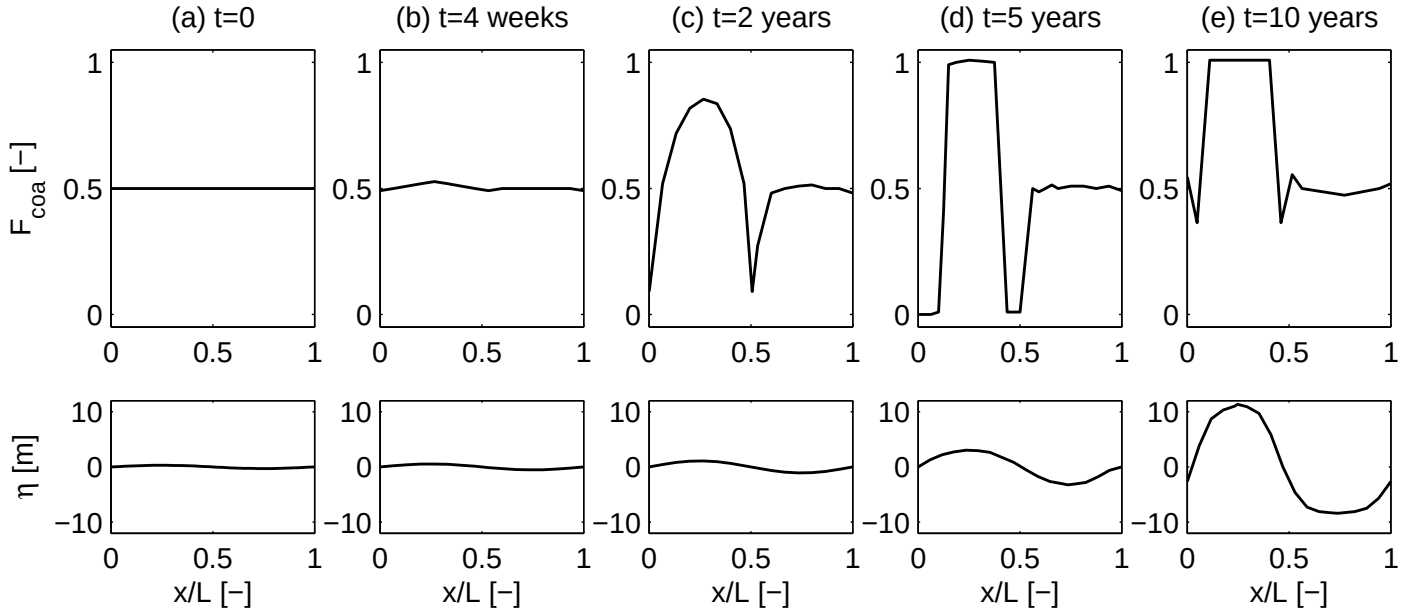

Figure 4: Evolution of the coarse grain fraction F_{coa} in the active layer (top) as well as the cross-sectional sandwave morphology η (bottom). Both quantities are plotted against the spatial coordinate x/L, at different times: (a) initial state with uniform fractions and small bed amplitude, (b) 4 weeks, (c) 2 years, (d) 5 years, (e) 10 years. Note: $F_{\text{fi}} = 1 - F_{\text{coa}}$.

tion 2. Initially, the active layer and the substrate are both assumed perfectly mixed, with the coarse and fine fraction equally present: $F_{\text{coa}} = F_{\text{fi}} = \frac{1}{2}$ and $F_{\text{substr,coa}} = F_{\text{substr,fi}} = \frac{1}{2}$. The mean grain size thus equals $D_{\text{m}} = 300$ μm. The active layer thickness is given by $\delta = 5D_{\text{coa}}$ (here: 2 mm).

As shown by Figure 4, a sandwave evolves, starting from a sinusoidal shape and then gradually deforming towards an equilibrium profile. This profile has a peaked and relatively narrow crest (about 12 m high), compared to the flattened and relatively wide trough (about 8 m below mean bed level). The growth of the sandwave is accompanied by a continuous redistribution of fine and coarse grains. The concentration of coarse grains increases at the crests, reaching its maximum of $F_{\text{coa}} = 1$ after about four years. The trough remains well-mixed, nearly identical to the sediment composition of the substrate.

After about 10 years, the simulation collapses after displaying instabilities at the transition point between erosion and deposition of the evolving sandwave (see Section 5.1). The simulation suggests that, although the sandwave shape hardly changes, a redistribution of fine and coarse grains is then taking place in the trough. Therefore, an equilibrium state is not reached.

4.3 *Simulation with uniform sediment*

In a second simulation, the sediment in the active layer and substrate consists of a single class ($N = 1$) with grain size equal to the mean grain size of the previous run: $D_1 = 300$ μm. Trivially, $D_{\text{m}} = D_1$ and the volume fraction equals 1, for all x and t. In this case, there is effectively no distinction between the active layer and the substrate, so the layer thickness δ has no meaning here. Hiding-exposure effects are absent, and Egiazaroff's (1965) hiding-exposure formula (6) indeed reduces to $\xi_1 = 1$. In this uniform case, sorting phenomena clearly cannot take place.

The sandwave evolves nearly identically to the simulation in Section 4.1, i.e. leading to a similar sandwave shape. Comparing the bimodal case presented in Section 4.1 to this result, the heterogeneity of the sediment apparently does not affect the shape of the sandwave.

4.4 *Sensitivity to sediment composition*

From additional simulations not further detailed here, we report the following observations (details in Wientjes 2006).

1. Reducing the difference between the grain sizes, while keeping the mean D_m constant, slows down the sorting process. However, the qualitative behaviour is the same as before in Section 4.2.

2. Taking larger grain sizes, while keeping the difference $D_{\text{coa}} - D_{\text{fi}}$ constant, produces the same qualitative tendency as the reference run in Section 4.2, with coarse grains accumulating at the crest. The initial redistribution of fine and coarse grains, however, may show differences.

3. Simulations without hiding-exposure, i.e. taking $\xi_j = 1$, show the same qualitative behaviour, but more pronounced and quicker coarsening of the sandwave crest.

4. Increasing the value of the active layer thick-

ness slows down the rearrangement of coarse and fine grains over the sandwave.

5. Changing the volume fractions in both the active layer (the initial situation) and the substrate does not lead to large differences.

6. Finally, when adopting three sediment classes ($N = 3$) instead of two, the qualitative picture remains the same. Coarse grains accumulate at the crest, where the concentration of intermediate and fine grains becomes zero.

5 DISCUSSION

5.1 *Grain sorting in the model results*

The inclusion of non-uniform sediment in the code by Van den Berg and Van Damme (2005) leads to sorting patterns over a (growing) sandwave. Qualitatively, the occurrence of the sorting pattern in the model results is caused by the fractional transport of different grain size classes; see the transport formula (5). The quantitative properties of the sorting process depend on several elements: the active layer thickness δ, the hiding-exposure mechanism and the sediment composition (to be discussed below in Section 5.2).

In the simulations, we distinguish two subsequent redistribution processes of coarse and fine grains. As the sandwave grows, coarse grains accumulate at the crest where $F_{\text{coa}} \to 1$ and where the finer grains completely disappear: $F_{\text{fi}} \downarrow 0$. Furthermore, as the trough gets deeper over time, sediment from the substrate enters the active layer. This explains why, during large parts of the simulations, the sediment composition in the active layer in the trough is identical to that of the substrate. However, when the tidal sandwave has nearly reached a final shape, the erosion-induced vertical exchange decreases. The simulations then display a second redistribution process, associated with the fractional sediment transport over a trough that no longer deepens and leading to a slight increase in the volume fraction of fine grains in the active layer in the trough.

An unfavourable property is the collapse of the simulations when this second redistribution process has started. This means that, with the present model results, we cannot investigate the grain size distribution over tidal sandwaves in a final morphodynamic equilibrium. In fact, the existence of such an equilibrium state is not guaranteed.

Crucial in the modelling approach is that the wavelength L of the sandwave is chosen such that the initial sandwave growth is largest ('fastest growing mode', see Section 4.1). As it turns out, the value of the preferred wavelength L is hardly affected by the inclusion of a bimodal mixture. Only with large differences in grain sizes (that we consider unrealistic in view of the observations reported in Section 2), the preferred wavelength L may shift to a different value. Also the shape and height of the sandwave are hardly affected by the change from uniform to non-uniform sediment.

5.2 *Active layer thickness, hiding-exposure and bimodal mixture*

The value of the active layer thickness δ affects the time scale of the sorting process. This result can be understood by combining equations (2) and (4) into

$$\frac{\partial F_j}{\partial t} = \frac{1}{\delta(1-p)} \left[F_{\text{vert},j} \frac{\partial \langle q_{\text{tot}} \rangle}{\partial x} - \frac{\partial \langle q_j \rangle}{\partial x} \right]. \quad (8)$$

The evolution of the volume fraction $\partial F_j / \partial t$ is thus proportional to δ^{-1}, explaining why a larger δ slows down the sorting process (and why a smaller δ speeds up this process). We have chosen the active layer thickness equal to $5D_{\text{coa}}$, i.e. five times the coarse grain size. From a physical point of view, the interface between the active layer and the substrate is not very strictly defined. Therefore, and also in view of the uncertainty in the sediment transport, we feel that there is some freedom in choosing the value of δ.

The simulations without Egiazaroff's (1965) hiding-exposure correction display a quicker evolution of the volume fractions. Indeed, as can be seen from equations (5) and (6) in Section 3.4, hiding-exposure reduces the difference between the critical shear stresses of the two fractions.

In this study, we have considered a bimodal mixture, which is in fact the most straightforward way of introducing heterogeneity to the sediment. Further increasing the complexity of the sediment mixture (considering a trimodal mixture) does not introduce new elements to the results. We therefore feel that the main qualitative properties of the sandwave model for non-uniform sediment are already captured when considering bimodal sediment.

5.3 *Comparison to observations*

In comparison to the observations, we first make the following remarks. Realistic grain sizes of the bimodal sediment mixture (see Table 1) were chosen in the model runs. Moreover, the wavelength selected by the modelling approach is of the order of observed wavelengths. The model results, however, give sandwave heights that exceed the empirical values (Table 1). This discrepancy can have several causes: the flow conditions in the model not matching the local conditions at the five sites in the North Sea, the lacking of some physical processes like wind waves, and the uncertainties in the hydrodynamic and sediment transport modules. Furthermore, it should be noted that the model runs did not reach a morphodynamic equilibrium state, which is assumed to be the case in the North Sea, since sandwave shape and dimensions change only little in time (Van Dijk et al. 2006).

The model results qualitatively agree with sorting patterns over sandwaves in the North Sea, both showing a trend of coarser grains accumulating at the crests. Although the empirical sorting trend, as summarised in Section 2.3, is more subtle, the fraction of fines ($D < 63$ μm) is completely absent in bed samples taken at the sandwave crests.

Although increasing the number of grain size classes N does not change the qualitative properties of the model results, we believe that the use of a more realistic grain size distribution would allow a more detailed comparison between model results and observations. Indeed, when considering a larger number of classes, quantities such as the median grain size (D_{50}) and the sorting ratio (D_{60}/D_{10}) can be modelled in a meaningful way.

Model runs were done for symmetric tidal flow conditions, containing the dominant M2-tidal constituent only. As a result, the modelled sandwaves are also symmetric and they do not migrate. To better reproduce the asymmetric and migrating sandwaves (e.g., see Figure 1c), a more detailed representation of the site-specific tidal characteristics is required, including higher harmonics (such as an M4-component) and residual flow (M0). This asymmetry in the forcing is also likely to introduce an asymmetry in the modelled sorting patterns.

6 CONCLUSIONS

We have extended an existing sandwave simulation code to account for the presence and transport of non-uniform sediment. To this end, we have adopted Hirano's (1971) active layer approach and considered a fractional sediment transport module, involving hiding-exposure effects according to Egiazaroff's formula (1965). The model results, simulating a growing sandwave with a bimodal sediment mixture, indicate that coarse grains accumulate at the crest, whereas the trough remains mixed with both coarse and fine grains. Fractional transport turns out to explain the qualitative sorting trend in the results. The model results show qualitative agreement with detailed observations from various sites in the North Sea.

7 ACKNOWLEDGEMENTS

This work originates from I.G.M. Wientjes' master's thesis Civil Engineering & Management, University of Twente. Data were collected and corrected in collaboration with the Directorate North Sea, Dutch Public Works and Water Management (DNZ-RWS). This work contributes to the EU-project MESH (Mapping European Seabed Habitats, `http://www.searchmesh.net`) and partially received funding through INTERREG III B. This research is supported by the Technology Foundation STW, applied science division of NWO and the technology programme of the Ministry of Economic Affairs.

REFERENCES

Egiazaroff, I. V. (1965). Calculation of non-uniform sediment concentrations. *J. Hyd. Div. 91*(4), 225–248.

Hirano, M. (1971). River bed degradation with armouring. *Trans. Jap. Soc. Civ. Eng. 3*, 194–195.

Hulscher, S. J. M. H. (1996). Tidal-induced large-scale regular bed form patterns in a three-dimensional shallow water model. *J. Geophys. Res. 101*(C9), 20,727–20,744.

Németh, A. A., S. J. M. H. Hulscher, and R. M. J. Van Damme (2007). Modelling offshore sand wave evolution. *Cont. Shelf Res. 27*(5), 713–728.

Passchier, S. and M. G. Kleinhans (2005). Observations of sand waves, megaripples, and hummocks in the dutch coastal area and their relation to currents and combined flow conditions. *J. Geophys. Res. 110*(F04S15), doi:10.1029/2004JF000215.

Schüttenhelm, R. T. E. (2002). Grain-size variability and crest stability of a North Sea sandwave in space and time. TNO Report 02-219-B, Netherlands Institute of Applied Geosciences, Utrecht, The Netherlands.

Seminara, G. (1995). Effect of grain sorting on the formation of bedforms. *Appl. Mech. Rev. 48*(9), 549–563.

Soulsby, R. L. (1997). *Dynamics of marine sands*. London: Thomas Telford.

Van den Berg, J. and R. M. J. Van Damme (2005). Sand wave simulation on large domains. In G. Parker and M. H. Garcia (Eds.), *Proc RCEM'05*, Urbana, Illinois, pp. 991–997. IAHR: Taylor & Francis/Balkema.

Van Dijk, T. A. G. P., P. J. P. Egberts, J. H. Brouwer, and S. Van Heteren (2006, April). The mobility of sand waves: an analysis of the behaviour and interference of bedforms from empirical data. In *Proc. 8th Nederlands Aardwetenschappelijk Congres, Programme & Abstracts*, Veldhoven, The Netherlands.

Van Dijk, T. A. G. P. and M. G. Kleinhans (2005). Processes controlling the dynamics of compound sand waves in the North Sea. *J. Geophys. Res. 110*(F04S10), doi:10.1029/2004JF000173.

Van Rijn, L. C. (1993). *Principles of sediment transport in rivers, estuaries and coastal seas*. Amsterdam: Aqua Publ.

Wientjes, I. G. M. (2006, July). Grain size sorting over offshore sandwaves. CE&M Research Report 2006R-004/WEM-005, University of Twente, Enschede, The Netherlands.